Academic Journal of Science and Technology
ISSN: 2771-3032 | Vol. 7, No. 1, 2023

T-C20 Carbon: A Three-Dimensional Topological Carbon Allotrope Constructed from Zigzag Carbon Chains

Li Peng[1], Jiaren Yuan[2] and Yue-E Xie[1, *]

[1]School of Physics and Electronic Engineering, Jiangsu University, Zhenjiang 212013, China
[2]School of Physics and Materials Science, Nanchang University, Nanchang 330031, China
[*]Corresponding author. E-mail: Yueex@ujs.edu.cn

Abstract: Carbon materials have attracted much attention due to their excellent electronic structure and topological properties. By linking the zigzag carbon chains with carbon dimers, we propose a new stable three-dimensional (3D) carbon allotrope: T-C20 carbon. This carbon structure has four nodal lines in the Brillouin zone (BZ) protected by mirror symmetry. Moreover, T-C20 carbon exhibits strong anisotropic optical properties and strong absorption in the whole infrared, visible and ultraviolet regions, which is suitable for the broadband photodetector. Our research provides a new idea for the construction of novel 3D topological carbon allotropes.

Keywords: Carbon allotrope, Zigzag carbon chains, Topological semimetals, Optical properties.

1. Introduction

Topological semimetals (TSMs) have an extraordinary band structure with the conduction bands and valence bands crisscrossing near the Fermi level. A series of novel physical properties associated with a particular topological electronic state have been explored, such as topological surface states, Fermi arcs, or chiral anomaly.[1-3] Furthermore, TSMs are widely used in a variety of fields, including photodetectors, quantum state manipulation, topological field-effect quantum transistors, spintronics, and topological quantum computing.[4] Until now, the majority of research in these areas has focused on heavy metal topological materials with strong spin-orbit coupling (SOC). However, topological properties are also very plentiful in light element systems, such as carbon materials.

Carbon materials have transformed the electronic and optoelectronic industry due to their encouraging properties. One intriguing property of carbon is its ability to form a variety of allotropes[5] owing to its unique bonding properties via three different hybridization methods (sp, sp^2, and sp^3). In recent decades, various carbon allotropes have been reported, including fullerenes,[6] carbon nanotubes (CNTs) ,[7] graphene (GR) ,[8] and 3D T-carbon[9] and carbon honeycombs (CHC) .[10, 11] Carbon allotropes exhibit abundant electronic structures and topological properties due to their unique lattice structures and bonding characteristics. For instance, one-dimensional (1D) graphene nanoribbons (GNRs) exist symmetry-protected topological phases.[12] Graphene and 6,6,12-graphyne are topological semimetals[8, 13] with Dirac cones. With increasing dimensionality, 3D carbon structures have more structural types and topological phases than low-dimensional carbon structures. A series of topological phases have been reported in 3D carbon structures, such as Dirac/Weyl points,[14-16] nodal lines,[17-19] nodal rings/knots,[14, 20, 21] nodal chains/nets,[22, 23] nodal surfaces,[2, 24] nodal balls, and nodal tubes.[25] Hence, 3D carbon allotropes provide a perfect platform to investigate topological phases.

Since the inception of nanotechnology, many new low-dimensional carbon allotropes have been successfully synthesized in the experiment, for instance, zero-dimensional (0D) cyclo[18] carbon,[26] 1D carbine,[27] two-dimensional(2D) graphdiyne and biphenylene networks.[28] Likewise, numerous approaches are proposed to construct 3D carbon allotropes. For example, atomic layer stacking is an effective method for constructing 3D carbon allotropes. Graphite can be regarded as graphene stacking via van der Waals force. However, since the van der Waals force is a sort of weak interaction force, the out-plane performance is far worse than the in-plane one. For instance, the out-plane conductivity is only 1%[29] of that for the in-plane. The issue could be solved when carbon atoms are linked by covalent bonds. A series of new carbon material could be designed by inserting carbon bonds into specific unit cells.[30, 31] For example, Wang et al. propose yne-diamond (YD)[32] by inserting acetylenic linkers into cubic diamond. Connecting specific carbon structures with carbon bonds or carbon chains is also an effective method. For example, 3D carbon honeycombs is obtained[33] by connecting zigzag GNRs using a row of common carbon atoms or carbon dimers. The zigzag carbon chain possesses rich and unique electronic and topological properties and plays a vital role in many carbon systems. It is expected to obtain excellent topological properties in new carbon materials with zigzag carbon chains constructed using the above method.

In this paper, we constructed 3D T-C20 carbon by linking zigzag carbon chains with carbon dimers. The results demonstrate that T-C20 carbon with good dynamical, mechanical and thermal stability is a topological semimetal with four nodal lines protected by mirror symmetry in the BZ. The topological properties originate from the zigzag carbon chain by analyzing the electronic properties of the disassembled substructure. In addition, T-C20 carbon has optical anisotropy and strong absorption of broad spectrum, highlighting its potential applications in optoelectronic devices. Furthermore, the researches not only enrich the types of carbon materials but also provide new ideas for designing

3D topological carbon allotropes.

2. Computation Method

The calculation is performed using the Vienna Ab initio simulation package (VASP)[34] based on density functional theory (DFT). The interaction between the atomic core and valence electrons is described by projector augmented wave (PAW), and the cutoff energy of the plane-wave is 500 eV. The interactions between valance electrons and exchange-correlation functional were described by the generalized gradient approximation (GGA) in the Perdew-Burke-Ernzerhof (PBE) scheme.[35] The convergence criteria for electron self-consistent relaxation was 10^{-5} eV. The atomic positions are optimized utilizing the conjugate gradient method with the residual force less than 10^{-3} eV/atom. The BZ was sampled by a 9×9×7 *k*-grid mesh. The phonon spectrum and thermodynamic stability of the structures were calculated by the PHONONPY software[36] and ab initio molecular dynamics (AIMD) simulations,[37] respectively.

3. Results and Discussion

3.1. Structure and stability

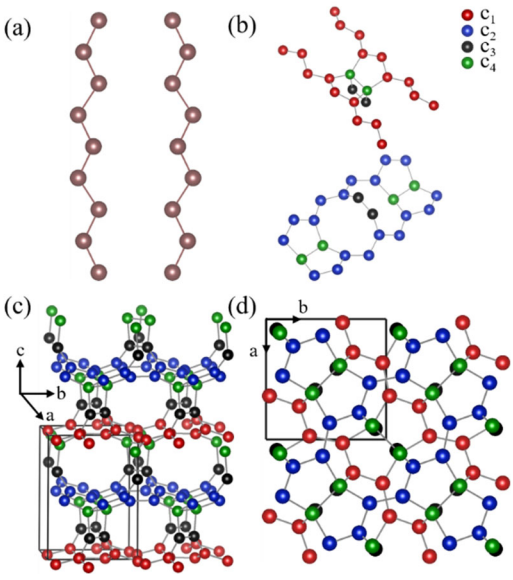

Figure 1. (a) A set of mirror-symmetric zigzag carbon chains. (b) Unequal planar structures constructed using Zigzag carbon chains (red atom C_1 and blue atom C_2) connected by carbon dimers (green atom C_4). (c) The side view of T-C20 carbon (the upper and lower 2D planar structures are connected with another carbon dimer (black atom C_3)). (d) The top view of the T-C20 carbon.

T-C20 carbon belongs to the space group P42NM (No.102) with lattice constants a=b=5.12 Å and c=7.09 Å. When a set of mirror-symmetric 1D zigzag carbon chains, as shown in Fig. 1(a), was connected with a green carbon dimer, two new orthogonal 2D wrinkled planar structures in Fig. 1(b) are constructed. The upper and lower orthogonal 2D wrinkled planar structures stack in AB form along the Z direction and are connected with another black carbon dimer, forming a new 3D structure T-C20 carbon. Consequently, T-C20 carbon is a combination of zigzag carbon chains and two types of carbon dimers. In which, red and blue zigzag carbon chain and black carbon dimer belong to sp^2 hybridization, while the green carbon dimer is sp^3 hybridization.

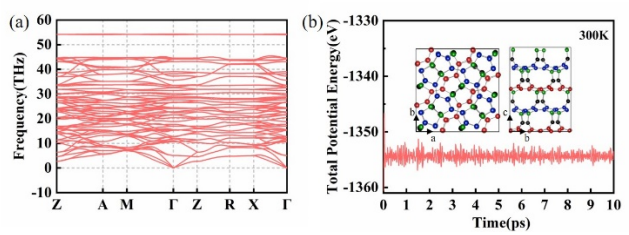

Figure 2. (a) Phonon dispersion of T-C20 carbon. (b) The total potential energy fluctuation of T-C20 carbon during AIMD simulation at 300K.Snapshots of the equilibrium structures of T-C20 carbon at temperatures of 300K after 10ps AIMD simulations are shown in the inset.

The cohesive energy of T-C20 carbon was evaluated to be -7.19 eV/atom, which is between graphite (-7.9 eV/atom) and T-carbon (-6.55 eV/atom), indicating T-C20 carbon may could be synthesized experimentally. Furthermore, the elastic constant tensor in the linear elastic region was calculated to analyze the mechanical stability. The elastic constants[38, 39] of T-C20 carbon are C_{11}=473 GPa, C_{12}=188 GPa, C_{13}=102 GPa, C_{33}=215 GPa, C_{44}=220 GPa, and C_{66}=67 GPa, which satisfy the Born stability criteria of the tetragonal crystal system: $C_{11}>|C_{12}|$, $2C_{13}^2 < C_{33}(C_{11}+C_{12})$, $C_{44}>0$ and $C_{66}>0$, demonstrating that T-C20 carbon is mechanically stable. The phonon spectrum of T-C20 carbon is also calculated with no imaginary frequency in the entire BZ, as shown in Fig. 2(a), which demonstrates that the proposed structure is dynamically stable. In the meantime, we assess the thermal stability of T-C20 carbon by AIMD simulation at 300 K in the framework of the canonical (NVT) ensemble. As shown in Fig. 2(b), the energy curve distribution is relatively stable within 10ps and the structure hold steady after 10ps. Hence, T-C20 carbon is dynamically, mechanically, and thermally stable.

3.2. Electronic properties

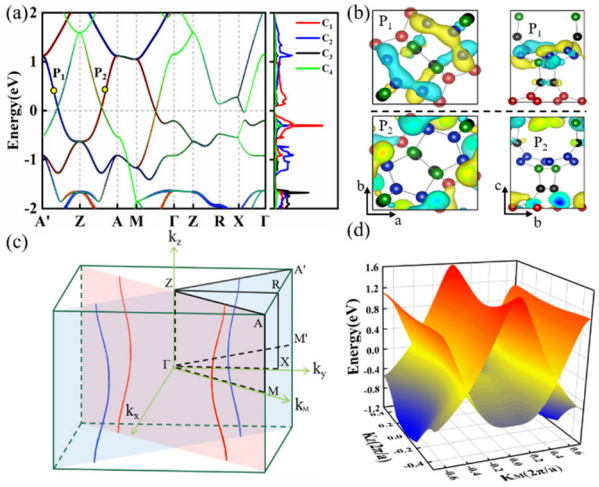

Figure 3. (a) The orbital-projected band structure of T-C20 carbon and the projected density of states of T-C20 carbon. (b) The top and side view of wave function of P_1 and P_2. (c) BZ and topological phase of T-C20 carbon. (d) 3D band structure of two mirror surfaces (pale pink and pale blue surfaces).

The orbital-projected band structure and projected density of states (PDOS) of T-C20 are shown in Fig. 3(a), the

conduction and valence bands of T-C20 carbon near the Fermi level crossover at the high-symmetry paths A'-Z, Z-A, and M-Γ, respectively. The PDOS represents that the electronic states of the structure near the Fermi level are approach zero, indicating T-C20 carbon is semimetal. In addition, the orbital-projected band structure shows that the crossing energy bands near the Fermi level are mainly contributed by C_1, C_2 atoms, and part of C_3 atoms, namely the states are mainly original from the orthogonal zigzag carbon chains.

Due to the symmetry of the structure, there are four nodal lines (red and blue curves) in the first BZ of T-C20 carbon, locating on two mutually orthogonal mirror surfaces (pale pink and pale blue surface) as shown in Fig. 3(c). The 3D band structure of the two mirror surfaces is exhibited in Fig. 3(d), a couple of slightly curved nodal lines are obtained by the upper and lower energy bands on the Fermi level, which is consistent with the nodal lines in Fig. 3(c). Due to the symmetry of T-C20 carbon, the node lines also have symmetry. The wave functions of the two crossing points P_1 and P_2 on the A'-Z and Z-A paths were calculated to explore the relation between topological phase and structure for T-C20 carbon. The electron distribution at point P_1 on the A'-Z path is mainly contributed from the red zigzag carbon chain in the description of Fig. 3(b). However, the point P_2 on the Z-A path is mostly from the blue zigzag carbon chain. Therefore, the red and blue nodal lines on two orthogonal mirror planes originate from two adjacent orthogonal red and blue planar structures in Fig. 1(b), respectively.

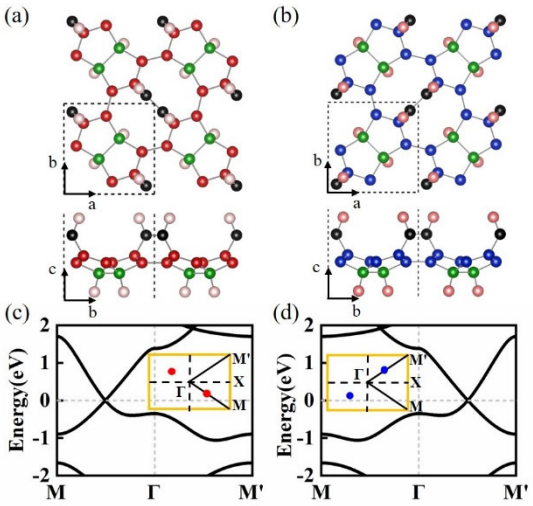

Figure 4. (a) Top view and side view of the passivated 2D structure mainly composed of red zigzag carbon chains (C_1 atoms). (b) The top and side views of the passivated 2D structure mainly composed of blue zigzag carbon chains (C_2 atoms), the light pink atoms are hydrogen atoms. (c) The band structure of substructure (a), the inset is its BZ and topological phase. (d) The band structure of the substructure (b), the inset is its BZ and topological phase.

T-C20 carbon can be split into two orthogonal 2D wrinkled planar structures as shown in Figs. 4(a) and 4(b). The structure was passivated with hydrogen atom. The electronic properties of the two substructures are investigated separately, and the band structures are shown in Figs. 4(c) and 4(d), respectively. The conduction and valence bands intersect at the Fermi level along the M-Γ and M'-Γ paths, respectively. The topological phase of the structure in the inset is obtained according to the symmetry with two nodal points (red) in the BZ as shown in Fig 4 (c). Additionally, the positions of the two red nodal points coincide with the red nodal line on the pale pink mirror surface as illustrated in Fig. 3(c). Similarly, the position of the blue nodal points corresponds to the light blue mirror surface. When the two 2D structures are AB stacked and construct 3D T-C20 carbon, the nodal points on the mirror surfaces spread into node lines along the Z direction on the mirror surfaces. Therefore, the nodal lines of T-C20 carbon are derived from the nodal point of the substructures.

3.3. Optical properties

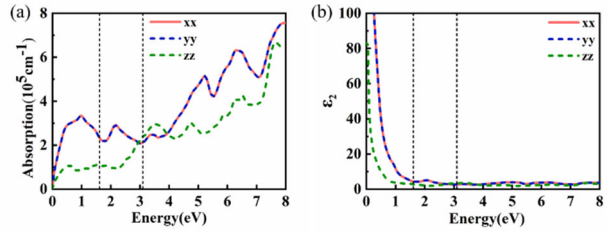

Figure 5. (a) Absorption coefficient spectrum of T-C20 carbon. (b) The imaginary part of the dielectric function of T-C20 carbon.

The optical properties are explored to analyze the potential application in optics. The absorption coefficient and the imaginary part of the dielectric function are calculated utilizing DFT. The frequency-dependent dielectric function is represented by $\varepsilon(\omega)=\varepsilon_1(\omega)+\mathrm{i}\varepsilon_2(\omega)$, where, $\varepsilon_1(\omega)$ and $\varepsilon_2(\omega)$ are the real and imaginary parts of the dielectric function, which is expressed by the following formulas:

$$\varepsilon_1(\omega)=1+\frac{2}{\pi}\mathrm{P}\int_0^{\infty}\frac{\omega'\varepsilon_2(\omega')}{\omega'^2-\omega^2}d\omega', \quad (1)$$

$$\varepsilon_2(\omega)=2\left(\frac{2\pi q}{\omega m}\right)^2\int|\boldsymbol{s}\cdot\boldsymbol{M}_{cv}(\boldsymbol{k})|^2\delta[E_c(\boldsymbol{k})-E_v(\boldsymbol{k})-\eta\omega]\frac{\mathrm{d}\boldsymbol{k}}{(2\pi)^3}, \quad (2)$$

where $\boldsymbol{M}_{cv}(\boldsymbol{k})$ is the momentum matrix element, $E_c(\boldsymbol{k})$ and $E_v(\boldsymbol{k})$ are the intrinsic energy levels in the conduction band and valence band, respectively. Furthermore, $\boldsymbol{s}$ is the unit vector, $\boldsymbol{k}$ is the wave vector, q is the charge quantity, ω and ω' are electromagnetic wave frequency, m is the mass of the free electron, δ factor represents the energy conservation relationship during the electron transition, P is the integral principal value. As shown in Fig. 5(a), both the absorption coefficient and the imaginary part of the dielectric function of T-C20 carbon have obvious anisotropy. The optical property is isotropic along the x and y directions and the optical property is anisotropy between the x/y and z directions. The anisotropy of optical properties is mainly caused by the structure anisotropic characteristics. The first absorption peaks appear at 1 eV and 0.6 eV in the x/y and z directions of the system, respectively. In most wavelength bands, the light absorption in the x/y plane is significantly stronger than that in the z-direction. Only in the range of 2.9 eV~3.9 eV, the in-plane absorption coefficient is slightly smaller than the out-of-plane absorption coefficient. The absorption coefficients in both directions reach the

exponential level of 10^5, which is comparable to organic perovskite solar or graphene.[40] However, unlike silicon and many other materials with very narrow wavelengths for the absorbed light, T-C20 carbon has a broad absorption range with strong absorption across the infrared, visible and ultraviolet regions. The carbon material exhibits excellent optical property, which could be used in photovoltaic solar cells and optoelectronic devices.

4. Conclusion

T-C20 carbon, a new 3D carbon allotrope, was constructed in this paper by connecting zigzag carbon chains with carbon dimers. The structure exhibits excellent thermodynamic, mechanical, and thermal stability. Based on ab initio calculations, the structural, electronic properties, and optical properties were investigated. The results show that T-C20 carbon is a topological semimetal with four symmetrical nodal lines. These nodal lines originate from 2D substructures constructed from zigzag carbon chains. Furthermore, T-C20 carbon has strong absorption in the whole infrared, visible and ultraviolet regions which is suitable for using in solar cells and optoelectronic devices. This paper not only provides new ideas for the construction of new topological carbon materials but also adds new materials for broad-spectrum optoelectronic devices.

Acknowledgment

Project supported by the National Natural Science Foundation of China (Grant No. 11874314, 51376005, 12074150 and 12004142) and Natural Science Funds for Colleges and Universities in Jiangsu Province (Grant No. 20KJB140017).

References

[1] Li J, Zhang Z, Wang C, Huang H, Gu B-L and Duan W 2020 Journal of Applied Physics 128 191101

[2] Wang J, Liu Y, Jin K-H, Sui X, Zhang L, Duan W, Liu F and Huang B 2018 Physical Review B 98 201112

[3] Wan X, Turner A M, Vishwanath A and Savrasov S Y 2011 Physical Review B 83 205101

[4] Cheng Y, Du J, Melnik R, Kawazoe Y and Wen B 2016 Carbon 98 468

[5] Chen Y, Xie Y, Yan X, Cohen M L and Zhang S 2020 Physics Reports 868 1

[6] Kroto H W, Heath J R, O'Brien S C, Curl R F and Smalley R E 1985 Nature 318 162

[7] Iijima S 1991 Nature 354 56

[8] Novoselov K S, Geim A K, Morozov S V, Jiang D, Zhang Y, Dubonos S V, Grigorieva I V and Firsov A A 2004 Science 306 666

[9] Sheng X-L, Yan Q-B, Ye F, Zheng Q-R and Su G 2011 Physical Review Letters 106 155703

[10] Krainyukova N V and Zubarev E N 2016 Physical Review Letters 116 055501

[11] Zhang J, Wang R, Zhu X, Pan A, Han C, Li X, Zhao D, Ma C, Wang W and Su H 2017 Nature Communications 8 683

[12] Rizzo D J, Veber G, Cao T, Bronner C, Chen T, Zhao F, Rodriguez H, Louie S G, Crommie M F and Fischer F R 2018 Nature 560 204

[13] Gao X, Liu H, Wang D and Zhang J 2019 Chemical Society Reviews 48 908

[14] Chen Y, Xie Y, Yang S A, Pan H, Zhang F, Cohen M L and Zhang S 2015 Nano Letters 15 6974

[15] Wu W, Xie Y and Chen Y 2021 Physical Review Materials 5 104201

[16] Zhang C, Ding X-Y, Gan L-Y, Cao Y, Li B-S, Wu X and Wang R 2020 Physical Review B 101 235119

[17] Bu K, Wang J-T, Weng H and Chen C 2020 Physical Review B 101 205104

[18] Zhao Z, Zhang Z and Guo W 2020 Journal of Materials Chemistry C 8 1548

[19] Li Z-Z, Chen J, Nie S, Xu L, Mizuseki H, Weng H and Wang J-T 2018 Carbon 133 39

[20] Zhao Z, Hang Y, Zhang Z and Guo W 2019 Physical Review B 100 115420

[21] Gao Y, Chen Y, Xie Y, Chang P-Y, Cohen M L and Zhang S 2018 Physical Review B 97 121108

[22] Bu K, Qian Y, Wang J-T and Weng H 2021 Physical Review B 103 L081108

[23] Zhang P, Ouyang T, Li J, He C, Chen Y, Zhang C, Tang C and Zhong J 2021 Nanotechnology 32 485705

[24] Zhong C, Chen Y, Xie Y, Yang S A, Cohen M L and Zhang S 2016 Nanoscale 8 7232

[25] Chen S-Z, Li S, Chen Y and Duan W 2020 Nano Letters 20 5400

[26] Kaiser K, Scriven L M, Schulz F, Gawel P, Gross L and Anderson H L 2019 Science 365 1299

[27] Pan B, Xiao J, Li J, Liu P, Wang C and Yang G 2015 Science Advances 1 e1500857

[28] Fan Q, Yan L, Tripp M W, Krejčí O, Dimosthenous S, Kachel S R, Chen M, Foster A S, Koert U, Liljeroth P and Gottfried J M 2021 Science 372 852

[29] Sugihara K and Sato H 1963 Journal of the Physical Society of Japan 18 332

[30] Wang J-T, Nie S, Weng H, Kawazoe Y and Chen C 2018 Physical Review Letters 120 026402

[31] Baughman R H, Eckhardt H and Kertesz M 1987 The Journal of Chemical Physics 87 6687

[32] Wang J-T, Chen C, Mizuseki H and Kawazoe Y 2018 Physical Chemistry Chemical Physics 20 7962

[33] Zhong C, Chen Y, Xie Y, Yang S A, Cohen M L and Zhang S B 2016 Nanoscale 8 7232

[34] Kresse G and Furthmüller J 1996 Physical Review B 54 11169

[35] Perdew J P, Chevary J A, Vosko S H, Jackson K A, Pederson M R, Singh D J and Fiolhais C 1992 Physical Review B 46 6671

[36] Togo A, Oba F and Tanaka I 2008 Physical Review B 78 147

[37] Nosé S 1984 The Journal of Chemical Physics 81 511

[38] Wu Z-j, Zhao E-j, Xiang H-p, Hao X-f, Liu X-j and Meng J 2007 Physical Review B 76 054115

[39] Mouhat F and Coudert F-X 2014 Physical Review B 90 224104

[40] Wang X, Zhi L and Müllen K 2008 Nano Letters 8 323